

LATERAL TORSIONAL BUCKLING OF WELDED STAINLESS STEEL I-PROFILE BEAMS: DESIGN AND RELIABILITY

Maarten FORTAN^a and Barbara ROSSI^{a,b}

^a Department of Civil Engineering, KU Leuven, Belgium

Jan Pieter de Nayerlaan 5, Sint-Katelijne-Waver, Belgium.

Email: maarten.fortan@kuleuven.be

^b University of Oxford, Department of Engineering Science, UK

Emails: barbara.rossi@new.ox.ac.uk

Keywords: Stainless steel structures; Lateral torsional buckling; Reliability analysis.

Abstract. *In this paper, a geometrically and materially non-linear numerical model using ANSYS is validated against 13 lateral torsional buckling (LTB) experiments as well as experiments from the literature. A parametric study comprising 30 geometries with each 12 lengths in the slenderness range of 0.35 to 1.95 is then performed. This numerical study is repeated for the stainless steel ferritic EN 1.4016, austenitic EN 1.4404 and duplex EN 1.4462 grades to ensure a safe design for all stainless steel families used in civil engineering structures. When compared to the numerical results, the current EN 1993-1-4 design rules are slightly unsafe for the intermediate slenderness range and increasingly conservative for stocky sections in the higher slenderness range. Based on this, the reliability assessment according to Annex D of EN 1990 leads to safety factors greater than the codified value of 1.1. However, by introducing the recent proposal of Taras and Greiner, improved predictions of the LTB strengths are achieved especially when the adjusted imperfection factors for each stainless steel family is used. Safe predictions are obtained in the intermediate slenderness range as well as high improvements of the prediction for stocky sections in the high slenderness range.*

22 1 INTRODUCTION

23 Stainless steel, as a Chromium-Nickel (Cr-Ni) alloy, has recently become a popular construction material
24 owing to the combination of excellent corrosion resistance and mechanical strength. In terms of their material
25 behaviour, a number of similarities exist between stainless steel and typical carbon steel, but sufficient differences
26 exist to necessitate specific treatment in design standards focused on structural applications. In the literature, these
27 differences are generally defined as the non-linear stress-strain curve with large strain hardening domain showed
28 by most stainless steel families as well as differences in conductivity and strength retention at high temperature.

29 The current European EN 1993-1-4 (2006) rules are in constant evolution. In the past decades, a lot of scientific
30 effort was spend on improving these design rules (SCI, 2017) and developing alternative design methods to
31 incorporate the benefits of strain hardening, such as the direct strength method and the continuous strength method
32 (Afshan and Gardner, 2013). However, compared to carbon steel or concrete, for stainless steel, some
33 improvements are still necessary to better tackle the material stress-strain curve influence on the structural
34 behaviour of components.

35 The current lateral torsional buckling (LTB) design rules for stainless steel beams are largely based on the
36 carbon steel ones and were validated against a very limited experimental basis, composed only of 24 experiments
37 on ferritic cold-formed channels spot welded back-to-back by Van Wyk et al. (1990) and 12 experiments on
38 welded stainless steel I-beams (Burgan et al., 2000 and Stangenberg, 2000). However more recently, 10 austenitic
39 experiments were published by Wang et al. (2014), including 6 experiments on doubly symmetrical I-section
40 beams and 4 beams with a wider tensile or compressive flange. That is the reason why, 13 experiments were
41 conducted by the authors of this paper, as described in (Fortan and Rossi, 2020), focusing on duplex stainless
42 steel. These experiments are used in this paper to validate a geometrically and materially non-linear numerical
43 model using ANSYS, which is then also compared to the previously cited reference experiments (Burgan et al.,
44 2000, Stangenberg, 2000 and Wang et al., 2014).

45 The validated numerical model is then used to perform a parametric study to assess the current design rules
46 for stainless steel and the proposed amendments by Taras and Greiner (2010) for carbon steel. Subsequently,
47 improvements to the design rules for stainless steel beams are proposed and confirmed by a reliability assessment.

2 DESIGN RULES

Comparison between the European EN 1993-1-4 (2006) and the American AISC (American Institute of Steel Construction) Design Guide 27 for structural stainless steel (Baddoo, 2013) is made in this chapter. Eurocode 3 is based on limit state design working with Ultimate Limit States (ULS) and Serviceability Limit States (SLS). Whereas the Load and Resistance Factor Design (LFRD) has replaced the Allowable Strength Design (ASD) in the AISC design rules. However, both methods are still used in the AISC guide. LFRD uses the resistance factor ϕ_b whereas ASD uses the safety factor Ω . To find the design strength, the following factors should be used for stainless steel members: $\phi_b=0.90$ (LFRD) and $\Omega = 1.67$ (ASD).

2.1 Eurocode

The design rules for LTB of stainless steel beams in EN 1993-1-4 (2006) are in essence those for carbon steel. The resistance $M_{b,Rd}$ is calculated by multiplying the moment resistance by the reduction factor χ_{LT} , see equations 1 to 4. This factor depends on the slenderness $\bar{\lambda}_{LT}$, the imperfection factor α_{LT} and the artificial plateau length $\bar{\lambda}_0$, the values of which, for welded I-sections, are presented in Table 1, where h is the clear height of the profile and b is its width.

$$\bar{\lambda}_{LT} = \sqrt{\frac{W_y f_y}{M_{cr}}} \quad (1)$$

$$\phi_{LT} = 0.5[1 + \alpha_{LT}(\bar{\lambda}_{LT} - \bar{\lambda}_0) + \bar{\lambda}_{LT}^2] \quad (2)$$

$$\chi_{LT} = \frac{1}{\phi_{LT} + \sqrt{\phi_{LT}^2 - \bar{\lambda}_{LT}^2}} \leq 1.0 \quad (3)$$

$$M_{b,Rd} = \chi_{LT} \frac{W_y f_y}{\gamma_{M1}} \quad (4)$$

where W_y is the section modulus taking into account the cross-section class and M_{cr} is the elastic critical moment for LTB. For stainless steel, due to the non-linear stress-strain behaviour, the yield strength f_y is defined as the 0.2% proof stress.

Improvements to these design rules were proposed in (Taras and Greiner, 2010) and (Taras, 2011), and will be integrated in the next revision of EN 1993-1-1 (2005) for carbon steel. The proposed changes, provided in equation 5, compensate for unsafe predictions in the low slenderness range and for the conservative strengths of stocky sections in their higher slenderness range. The main difference proposed in (Taras and Greiner, 2010) is the inclusion of the normalized slenderness for weak axis flexural buckling for the unstiffened length of the compression flange $\bar{\lambda}_z$ and the square root of the strong-to-weak axis moment resistance ratio, see equation 5 which replaces equation 2 in the design. For welded cross-sections, the imperfection factor α_{LT} is 0.21 and the factor $\alpha_{LT}\sqrt{W_{y,el}/W_{z,el}}$ is limited to 0.64.

$$\phi_{LT} = 0.5 \left[1 + \alpha_{LT}(\bar{\lambda}_z - \bar{\lambda}_0) \sqrt{\frac{W_{y,el}}{W_{z,el}} \frac{\bar{\lambda}_{LT}^2}{\bar{\lambda}_z^2}} + \bar{\lambda}_{LT}^2 \right] \quad (5)$$

2.2 AISC

Supplementary design rules for structural stainless steel are specified in the Design Guide 27 for structural stainless steel (Baddoo, 2013). In this paper, all cross-sections are doubly symmetric I-shaped members with compact webs and therefore equations 6 to 9 apply. A unified variable notation was herein adopted for comparison purposes. When the flanges are noncompact or slender, one additional check for compression flange local buckling has to be performed.

$$M_n = C_b \left[M_p - (M_p - 0.45f_y W_{el,y}) \left(\frac{L_b - L_p}{L_r - L_p} \right) \right] \leq M_p \quad \text{When } L_p < L_b < L_r \quad (6)$$

$$M_n = 0.64f_{cr} W_{el,y} \leq M_p \quad \text{When } L_r < L_b \quad (7)$$

$$L_p = 0.8r_z \sqrt{\frac{E}{f_y}} \quad (8)$$

$$L_r = 1.95r_{ts} \frac{E}{0.7f_y} \sqrt{\frac{I_t}{W_{el,y}h_0} + \sqrt{\left(\frac{I_t}{W_{el,y}h_0} \right)^2 + 6.76 \left(\frac{0.7f_y}{E} \right)^2}} \quad (9)$$

where M_n is the nominal flexural strength, M_p is the plastic bending moment, f_{cr} is the critical stress, r_z is the radius of gyration for the weak axis, r_{ts} is the effective radius of gyration, and h_0 is the distance between the flange

centroids. L_b is defined as the length between points that are either braced against lateral displacement of the compression flange or braced against twist of the cross section.

3 NUMERICAL ANALYSIS

3.1 Validation against tests from (Fortan and Rossi, 2020)

In (Fortan and Rossi, 2020), 13 LTB experiments are described. They include tests on three different stainless steel grades covering a slenderness range from 0.30 to 0.76. The tests comprise four different cross-section geometries, with approximately the same weak axis bending resistance, and various lengths per cross-section. The beams were tested in a four-point bending test set-up with fork-end like support conditions and lateral supports at the loading points. The displacements at the loading points and supports were measured with LVDTs, while, along the buckling length of the beam, in between the lateral supports, the displacements in flexure and torsion were measured using a series of inclinometers along the web combined with stereo vision digital image correlation (DIC) recoding the displacement field of a black and white speckle pattern painted onto the beam.

Presently, a finite element (FE) model representing these tests was developed in ANSYS using quadratic shell elements SHELL281. The mesh size was selected based on a sensitivity analysis (i.e. the optimal mesh size at which the obtained results became insensitive to further mesh refinement, while sustaining a compromise between computational time and numerical convergence). The material implemented in the model is the true strain measurements obtained with DIC versus the true stress in a multilinear isotropic hardening model (MISO). The differences between the rolling and transverse directions material behaviours were neglected. Since the rolling direction is the most critical and corresponds to the length direction of the flanges, the material model matches the uniaxial tensile tests in this direction.

The residual stresses and geometrical imperfections were modelled separately. Since no residual stress measurements were taken during these experiments, the residual stress model for stainless steel welded beams presented in (Yuan et al., 2014) was introduced in the FE model using the INISTATE command. Extra nodes were created in the transition from tensile to compressive stresses to ensure a smooth transition. The geometrical imperfections were introduced using the first eigenmode shape obtained from a modal analysis of the beams,

115 corresponding to a bow imperfection around the weak axis of the beam. The measured imperfection, see (Fortan
116 and Rossi, 2020), was used to scale the first eigenmode obtained numerically along the buckling length of the
117 beam.

118 The vertical displacement at the fork-end supports was constrained in the FE model and a rigid region was
119 created in a range of 100 mm around this support, which corresponds to the bottom plate of the fork-end supports,
120 shown in Figure 1. This rigid region is allowed to rotate but its deformations are controlled by a master node,
121 creating a hinge at this point. Furthermore, both flanges are constrained to move sideways therefore blocking
122 rotation around the longitudinal axis. At the loading points, the load is applied in the centre node of the flange. A
123 rigid region, over the width of the flange, is created. A master node on its centre controls its vertical displacements
124 and rotations, mimicking the effect of the rolls used to transfer the load to the beam during the experiments. At
125 the loading points, a lateral constraint is added to the side of the stiffener. It copies the effect of the lateral sliding
126 supports used during the experiments.

127 During the tests, quite large rotations (up to 1°) were measured at the loading points for four specimens
128 I160x160Lb1800_EN1.4162, I263x161Lb2000_EN1.4062, I260x160Lb2800_EN1.4162 and
129 I212x160Lb2000_EN1.4062. They indicate that, for these specimens, the lateral supports were not perfectly
130 aligned with the stiffener. In the FE model, the location was slightly varied in order to tackle these differences
131 individually. An example is given in Figure 2 for the specimen I263x161Lb2000_EN1.4062, comparing the
132 measured rotations at the level of each loading point and in the middle of the beam to the numerically obtained
133 ones. For most beams, a good match between the FEM and the experiment was found. However, specimens for
134 which a very large initial imperfection amplitude was measured, showed less accurate predictions of the rotations
135 at the loading points. For I160x160Lb1500_EN1.4162, the right lateral support was not modelled to match the
136 asymmetrical buckling failure mode seen in the experiment.

137 When comparing the numerically obtained ultimate loads to the experimental ones, see Table 2, a very good
138 correlation was found, with an average FEM-to-test strength ratio of 0.991 and a coefficient of variation (COV)
139 of 0.019. Furthermore, the stiffness of the beams matches well the simulated ones, as can be seen in Figure 3. A
140 slightly worse match was found for two sections with a height h of 160 mm. The ultimate loads of these sections

141 were still well predicted, but their numerical post-buckling behaviours and stiffnesses close to the ultimate load
142 were not perfectly modelled although still in the acceptable domain. This is possibly caused by a change in residual
143 stresses for this section compared to the used model. Furthermore, when comparing the out-of-plane
144 displacements measured with DIC to the displacements of the FE model, see Figure 4 and Figure 5, some slight
145 discrepancy was noticed. This shift was caused by a movement of the lateral supports during the experiments.
146 However, the rotations, bending stiffnesses and resistances were still very well predicted by the numerical
147 simulations. Based on this comparison, one can conclude that the model is able to finely represent the buckling
148 behaviour of the tested beams.

149 **3.2 Validation against tests from the literature**

150 In the context of the further development of EN 1993-1-4, (Burgan et al., 2000) and (Stangenberg, 2000) tested
151 12 specimens in a four-point bending test configuration, including 9 specimens made of the austenitic grade EN
152 1.4301 and 3 specimens made of the duplex grade EN 1.4462. Similar to (Fortan and Rossi, 2020), different cross-
153 section sizes were tested with different buckling lengths. However, no lateral supports were used in the four-point
154 bending tests, but instead, extra plates were welded to both sides of the section, in the shear spans, greatly
155 increasing their shear capacity and torsional stiffness. In addition, endplates were welded to both ends of the beam,
156 restraining warping of both end cross-sections. The endplates were used as fork-end supports with a vertical
157 support on the bottom and lateral supports on each sides of the section.

158 The FE models used to validate these tests are similar to the models presented in paragraph 3.1, but with fork-
159 end supports and no lateral supports. The material model is the measured true stress true strain curve of the
160 material described in (Stangenberg, 2000). Since no imperfections were measured, the first eigenmode was
161 rescaled to an amplitude of $L/1000$, and the residual stress model of (Yuan et al., 2014) was used. A comparison
162 of the failure loads from the test and the corresponding FEMs is given in Table 3. A good correlation was found
163 with an average FEM-to- test strengths of 1.02 and a COV of 0.044.

164 More recently, an experimental study by Wang et al. (2014) on 10 austenitic stainless steel beams suffering
165 LTB was published. The beams were divided in 3 groups: 6 beams with a biaxial symmetrical I-section, 2 beams
166 with a wider tension flange and 2 beams with a wider compression flange. The study also included material tensile

167 tests, and measurements of the residual stress and geometrical imperfections. The four-point bending tests were
168 performed with fork-end supports, but without extra lateral supports at the loading points. During the test, the
169 displacements were measured using LVDTs and strains were measured with 10 strain gauges placed at mid-span,
170 both on the web and flanges.

171 For the validation, the 6 biaxial symmetrical sections were presently modelled. The geometrical imperfections
172 were introduced by re-scaling the first eigenmode with the measured imperfection. The residual stresses measured
173 in the study are in good agreement with the model of (Yuan et al., 2014). Therefore, this model was used instead
174 of the model proposed by Wang et al. (2014). In Table 4, an overview of the failure loads obtained experimentally
175 and numerically is given.

176 In addition, the initial stiffnesses of each experiment were compared to the ones of the FEMs for the vertical
177 mid-span displacement, see Figure 6. While the beams EI1, EI2 and EI3 match the FEM results quite well, the
178 beams EI4, EI5 and EI6 show a discrepancy in their initial stiffness. Since the initial numerical stiffness is
179 controlled by the material law, the cross-section properties and the measured lengths, which were all taken from
180 (Wang et al., 2014), it was not possible to strive for a better agreement.

181 **3.3 Parametric study**

182 The design rules are presently assessed based on a parametric study of a welded beam with fork-end support
183 conditions submitted to pure bending. Similar to the previous models, quadratic SHELL281 elements were used.
184 The model uses symmetry to minimize time and computational effort by applying symmetry boundary
185 conditions on one end of the beam. On the other end, fork-end supports are created by applying a vertical
186 constraint to the top flange and lateral constraints to the edges of the top and bottom flanges. To avoid local
187 deformations at the end, multi point constraint (MPC) are used via CONTA176 and TARGE170 elements.
188 Separate MPCs are created for the web and flanges to allow free warping of the end cross-section.

189 The dimensions of the modelled sections are based on 30 hot-rolled I-profiles. Half of the sections have a
190 height-to-width ratio smaller than 2.0 and, within each half, the sections consist of 5 IPE, 5 HEA and 5 HEM
191 cross-sections. This distribution ensures a wide range of cross-section geometries, with different ratios between

192 the strong and weak axis bending elastic section moduli, which is the most important amendment in the proposal
193 of (Taras and Greiner, 2010). For each profile, 12 slendernesses ranging between 0.3 and 1.95 were chosen to
194 cover a wide range of the LTB curves.

195 Three stainless steel families are integrated in EN 1993-1-4 (2006): ferritic, austenitic and duplex stainless
196 steels. For each family, one typical grade was chosen to run the full parametric study: EN 1.4016 as ferritic grade,
197 EN 1.4404 as austenitic grade and EN 1.4462 as duplex grade. The materials were included with nominal material
198 properties for hot-rolled plates, which complies with the recommendations of (SCI, 2017). An overview of the
199 used parameters is given in Table 5. The materials were modelled using the two-stage Ramberg-Osgood's model
200 as described in annex C of EN 1993-1-4 (2006), and afterwards integrated in the model using a multilinear
201 isotropic hardening model.

202 The geometrical imperfections were integrated using the first eigenmode obtained from the modal analysis as
203 imperfection shape with a scaled amplitude equal to $L/1000$, similar to (Taras, 2011). This eigenmode for a beam
204 with fork-end supports corresponds to a weak axis flexure bow imperfection combined with, for the smallest
205 lengths, some distortion of the web. The residual stresses were induced using the INISTATE command and they
206 are in agreement with the model of Yuan et al. (2014). This model leads to no difference between the stainless
207 steel families regarding the shape of the residual stresses, but the austenitic stainless steels show a higher
208 amplitude for the tensile stresses in the vicinity of the weld, corresponding to 80% of the yield strength, where
209 the ferritic and duplex stainless steels have maximum tensile stresses corresponding to 60% of the yield strength.
210 An overview of the numerical results is shown in Figure 7, with comparisons to the current buckling curve
211 proposed in EN 1993-1-4 (2006).

212 **4 ASSESSMENT OF THE DESIGN RULES**

213 **4.1 New proposal**

214 The numerical results are here used to assess the current design rules prescribed in EN 1993-1-4 (2006).
215 Furthermore, since the proposal by Taras and Greiner (2010) showed promising results in (Fortan and Rossi,
216 2020) and (Fortan et al., 2016) for stainless steels, the simulations are also compared to this proposal. However,

the non-linearity of the stress-strain curve and the different residual stresses influence the LTB behaviour of the stainless steel beams. Therefore, a separate imperfection factor α_{LT} will be determined for stainless steel. Since the non-linearity and residual stresses vary over the different stainless steel families, it will be determined for each family. The imperfection factor α_{LT} is influenced by the corresponding plateau length $\bar{\lambda}_0$, which is currently 0.4 in EN 1993-1-4 but 0.2 in EN 1993-1-1 and, in the proposal of Taras and Greiner. Therefore, the plateau length will be varied between 0.2, 0.3 and 0.4 to determine the optimal plateau length for stainless steel.

The imperfection factor α_{LT} is then calculated based on the numerical results. Since all design parameters as well as ultimate resistances are known, the only unknowns are the imperfection factor α_{LT} and plateau length $\bar{\lambda}_0$. Therefore, for each model, an imperfection factor is determined per fixed plateau length (0.2, 0.3 or 0.4), and the average and standard deviation are calculated, see Table 6. Since the standard deviation is relatively large compared to the imperfection factor α_{LT} , using the average value to draw conclusions would lead to unsafe predictions. Therefore, the proposed imperfection factor α_{LT} corresponds to the 5% upper fractile.

Based on this, for each family, one can conclude that both the average and the standard deviation of the imperfection factor are minimal for a plateau length of 0.2. When the proposed imperfection factors are used to predict the LTB resistances, a plateau length of 0.2 also leads to the lowest averages ratio and COVs, see Table 6. Furthermore, the COVs of the predictions are similar for all stainless steel families, but small differences are noticed in the predictions of the averages. It is hence proposed to use a plateau length $\bar{\lambda}_0$ equal to 0.2 for all stainless steel families, using equation 5, in combination with the following imperfection factors α_{LT} per family: 0.27 for ferritic stainless steels, 0.37 for austenitic stainless steels and 0.23 for duplex stainless steels.

Figure 8 provides a comparison of the design rules of EN1993-1-4, the proposal from Taras and Greiner and the adaption with the proposed imperfection factors α_{LT} per stainless steel family and the plateau length $\bar{\lambda}_0$ of 0.2. The current design rules for stainless steel show similar differences as the ones observed for carbon steel, as described in (Taras, 2011). In the low slenderness range, around 0.5, unsafe predictions are found, while, in the higher slenderness range, above 1.0, the predictions are quite conservative with ratios between the failure loads and the predicted ones higher than 1.5. This is valid for all stainless steel families since it is mainly caused by the cross-section geometrical properties. The scatter on the predictions is significantly reduced using the equation

243 proposed by Taras and Greiner. However, some unsafe predictions are visible mainly because the initial proposal
244 was calibrated for carbon steel rather than for stainless steel. This effect is primarily noticeable for the austenitic
245 family due to the higher residual stresses and the rounder stress-strain curve compared to the ferritic and duplex
246 stainless steel families. Last, the proposed combination of the imperfection factors α_{LT} per stainless steel family
247 and the plateau length $\bar{\lambda}_0$ of 0.2 leads to very consistent predictions of the failure loads for all the stainless steel
248 families and slenderness range. Slightly unsafe predictions can rarely be pointed out and the scatter is comparable
249 to the one of the unmodified proposal of Taras and Greiner. The ratio between the numerically obtained failure
250 loads and the theoretical predictions is also more constant and compact, over the whole slenderness range. In the
251 higher slenderness range, predictions are up to 40% better for duplex and ferritic stainless steels. For austenitic
252 stainless steels, improved predictions, up to 30% better, are obtained.

253 A similar trend can be noticed for the design rules specified by AISC as depicted in Figure 9, with unsafe
254 predictions of the LTB resistance in the slenderness range i.e. from 0.5 to 1.2 and very high conservatism in the
255 high slenderness domain. The degree of conservatism as well as the overestimation are larger compared to the
256 predictions delivered by EN 1993-1-4. The proposed formula combined with the imperfection factors is clearly
257 more consistent for all stainless steel families with improved and safer predictions for slendernesses lower than
258 1.2 and a much less conservatism at higher slendernesses.

259 **4.2 Reliability assessment**

260 The reliability of the new proposal is checked based on the numerical data according to the methodology
261 described in Afshan et al. (2015), which is in agreement with the one provided in EN1990 annex D (2002). An
262 overview of the most important parameters is presented in Table 7. Due to the differences between the stainless
263 steel families and their LTB behaviours, the safety factor is determined separately for each family, since sufficient
264 data points were available for each subset. Furthermore, a safety factor evaluation for each of the previously
265 mentioned design rules is also made.

266 The COVs for the design parameters are based on (Afshan et al., 2015), where an extensive study of the
267 variabilities of stainless steel design parameters and resistances is provided. The COV of a stainless steel I-section

268 in bending is 0.05 independent of the used grade. However, the COV of the yield strength f_y was determined based
269 on a large number of tensile tests and proved to be dependent on the stainless steel family. Therefore, the used
270 coefficients of variations for the strength of the material were taken as 0.045 for ferritic stainless steel, 0.06 for
271 austenitic stainless steel and 0.03 for duplex stainless steel.

272 There are however some minor modifications in the approach to determine the parameters c and d for each
273 specific test. Following the methodology used by Afshan et al. (2015), the effect of the variation on the resistance
274 function is calculated using weighing factors. These weighing factors take into account that the effect of the yield
275 strength on the resistance in the high slenderness range is negligible, whereas the effect of the variability of the
276 geometry in this range is amplified. The weighing factors are determined by checking the influence of a small
277 increase in the considered variable on the resistance. However, in the proposal by Taras and Greiner, and for our
278 proposal for stainless steel, the effect of a small increase in the geometry cannot be obtained in a straightforward
279 way, due to the introduction of the slenderness for weak axis flexural buckling. Therefore, a cumulative increase
280 of the cross-sectional dimensions (height, width and thicknesses of the flanges separately) resulting in an increase
281 of 1.001 of the strong axis section modulus was used. This results in an individual weighing factor per model,
282 depending on the cross-section and slenderness.

283 In Table 7, an overview of the overstrength factor b and the variability on the strength function V_δ is given for
284 each data set. The current design rules in EN 1993-1-4 have overall the lowest overstrength factor. However, for
285 austenitic stainless steels, this factor is smaller than one, resulting in a global unsafe design. The COV V_δ ,
286 representing the scatter of the resistance function, is also high with values close to 10% for each family. The
287 combination of a low overstrength factor with a high COV leads to a very high safety factor of 1.50 for ferritic
288 stainless steels, 1.46 for austenitic stainless steels and 1.38 for duplex stainless steels compared to the codified
289 value which is 1.10 for stainless steel.

290 By introducing the extra parameters according to Taras and Greiner (2010), the COVs are greatly reduced,
291 resulting in a large decrease in the safety factor γ_{M1} . The safety factor is further reduced to acceptable values by
292 integrating the proposed imperfection factors and plateau length as previously developed.

293 The numerical analysis was done based on nominal material parameters, which give an extreme view on the
294 safety factors. In (Afshan et al., 2015), it is proven that, statistically, stainless steels show a certain overstrength
295 compared to the nominal values provided in the standard. Therefore, an overstrength factor on the material is
296 taken into account when determining the final safety factor. The overstrength factors presented by Afshan et al.
297 are 1.20 for ferritic stainless steels, 1.30 for austenitic stainless steels and 1.10 for duplex stainless steels and
298 correspond very well with the found overstrength in this study (Fortan and Rossi, 2020). Nevertheless, as
299 previously mentioned, the effect of the yield strength on the resistance function is not directly proportional.
300 Therefore, the overstrength factor is also taken into account using the weighing factor of the yield strength. This
301 results in a safety factor that is dependent on the slenderness of the beam: due to the larger impact of the
302 overstrength, we have a smaller safety factor for low slenderness's and, due to the negligible effect of the material
303 strength on these beams, we have a higher safety factor in the higher slenderness range. As a result, the minimal
304 and maximal safety factors including the overstrength factors are given in the last column of Table 7. Furthermore,
305 curves showing the variation of the safety factors with the slenderness of the beam for each stainless steel family
306 and each design rule are given in Figure 10. Due to the fact that the effect of the overstrength factor is negligible
307 at higher slenderness, and the fact that the safety factor excluding overstrength is nearly constant, it can be
308 concluded that the maximum safety factors presented in Table 7 are representative. Although the safety factors
309 for ferritic and duplex stainless steels slightly exceed the codified value of 1.10 in the higher slenderness range,
310 the authors believe that it is reliable to propose a safety factor γ_{M1} of 1.10 for all stainless steel families, due to the
311 clear overstrength of the models, right in this slenderness range, as can be seen in Figure 8.

312 An alternative proposal is also proposed in Table 7. To determine the imperfection factors, we ensured that (1)
313 a maximal safety factor including overstrength of exactly 1.10 was reached; and (2) a safe design for the covered
314 slenderness range in the parametric study was obtained. However, for the austenitic family, the safety factor
315 excluding overstrength reaches values close to 1.15 for beams with a slenderness higher than 1.95.

316 The reliability of the rules specified in the Design Guide 27 for AISC (Baddoo, 2013) were evaluated using
317 the methodology proposed in Appendix B of this guide, where the safety factor is evaluated using Equation 10.
318 The mean values of the random material M_m and fabrication factors F_m correspond to those specified in the
319 reliability analysis of the Eurocode. The corresponding variabilities are also used to calculate the COV V_R . It is

320 worth noting at this stage that this method does not include weighing factors to compensate the effect of the
 321 overstrength on the resistance function. The mean P_m of professional factor P , shown as the test-to-design strength
 322 ratio over the whole data set, has the effect of balancing the unsafe results in the low slenderness range and the
 323 conservative results in the high slenderness range. For a target reliability index β of 2.6 for structural stainless
 324 steel members, an overview of the safety factor for each family is given in Table 8. In this work, it is seen that the
 325 worst predictions were obtained for beams with a slenderness equal to 0.9, resulting in a minimal mean
 326 professional factor P_m of 0.89 for austenitic stainless steels. Therefore, in Table 9, an overview of the safety factor
 327 is given for the numerical models with a slenderness of 0.9, but using the weighing factor on the material factor
 328 M_m i.e. taking into account that the effect of the yield strength on the resistance in the high slenderness range is
 329 limited. That eventually leads to a more realistic value of the safety factor which appears to be ranging between
 330 0.89 for ferritic and duplex stainless steels and 0.87 for austenitic stainless steels. In general, it can be seen that
 331 the proposal leads to better predictions combined with greatly improved safety factors approaching 1.0 for ferritic
 332 and duplex stainless steels and 1.1 for austenitic stainless steels.

$$333 \quad \phi = \frac{1.481 M_m F_m P_m}{e^{\beta \sqrt{V_R^2 + V_Q^2}}} \quad (10)$$

334 5 CONCLUSION

335 In this paper, a geometrically and materially non-linear numerical model using ANSYS is validated against 13
 336 LTB experiments, as described in (Fortan and Rossi, 2020). The numerical model includes the measured true
 337 stress true strain material model and uses the first eigenmode, rescaled to the measured imperfection amplitudes,
 338 as geometrical imperfections. The residual stresses are added using the model proposed by Yuan et al. (2014).
 339 The FE models succeed in accurately predicting the experimental resistances with an average ratio between the
 340 experimental and numerical strengths of 0.991 and a COV of 0.019. The models also prove to accurately predict
 341 the vertical displacements and rotations at different positions along the tested beams. The numerical model is then
 342 further validated against the LTB experiments on stainless steel welded I-beams found in the literature (Burgan
 343 et al., 2000), (Stangenberg, 2000) and (Wang et al., 2014). The average FEM-to-test strength ratio corresponds to
 344 1.02 with a COV of 0.044 for (Burgan et al., 2000) and (Stangenberg, 2000) and an average ratio of 1.04 with a
 345 COV of 0.042 for (Wang et al., 2014).

Afterwards, an extensive parametric study including a ferritic, austenitic and duplex stainless steel grades is carried out. For each material, 30 cross-sections are modelled with 12 different buckling lengths resulting in a slenderness range of 0.3 to 1.95 for each cross-section and material. The numerical data is used to assess the current design rules provided in EN 1993-1-4 and the proposed design rules by Taras and Greiner (2010) for carbon steel. Based on this assessment, optimal plateau length $\bar{\lambda}_0$ and imperfection factors α_{LT} are derived for each stainless steel family. The proposed imperfection factors α_{LT} are: 0.27 for ferritic stainless steels, 0.37 for austenitic stainless steels and 0.23 for duplex stainless steels with a constant plateau length $\bar{\lambda}_0$ of 0.2 for all families, and without limitation of this factor in contrast to the proposal for carbon steel, where the factor $\alpha_{LT}\sqrt{W_{y,el}/W_{z,el}}$ is limited to 0.64. This proposal results in safer predictions of the LTB resistances in the medium slenderness range and greatly reduces the conservatism of the codified predictions for stocky sections in their high slenderness range.

A reliability analysis according to EN 1990 annex D is then performed. Due to the combination of a low overstrength factor, caused by unsafe results in the smaller slenderness range, and a high scatter in the higher slenderness range, very large safety factors (ranging between 1.13 and 1.45) are calculated for the current design rules proposed in EN 1993-1-4. On the contrary, one demonstrates that it is reliable to use Taras and Greiner's methodology together with the proposed optimum imperfection factors per stainless steel family and plateau length, in combination with a safety factor γ_{MI} of 1.10, for all stainless steels. However, this proposal leads to slightly conservative safety factor (of 1.06) for austenitic stainless steel. This can be solved by adopting the alternative proposal, where all safety factors are exactly 1.10. Therefore, the authors propose to include the following design rules (equations 11 to 14) in the next revisions of EN 1993-1-4 in combination with the parameters in Table 10 for a safer, more efficient and more consistent design.

The design rules specified by AISC (Baddoo, 2013) result in consistent unsafe predictions for beams with a slenderness lower than 1.2 and a large conservatism for beams with a higher slenderness. Similarly to the European design rules, the new proposal leads to more consistent and safer predictions for all families in the whole slenderness range, resulting in a safety factor between 1.05 and 1.28 according to the reliability analysis.

$$\lambda_{LT} = \sqrt{\frac{W_y f_y}{M_{cr}}} \quad (11)$$

$$\phi_{LT} = 0.5 \left[1 + \alpha_{LT} (\bar{\lambda}_z - \lambda_0) \sqrt{\frac{W_{y,el} \bar{\lambda}_{LT}^2}{W_{z,el} \bar{\lambda}_z^2} + \bar{\lambda}_{LT}^2} \right] \quad (12)$$

$$\chi_{LT} = \frac{1}{\phi_{LT} + \sqrt{\phi_{LT}^2 - \bar{\lambda}_{LT}^2}} \leq 1.0 \quad (13)$$

$$M_{b,Rd} = \chi_{LT} \frac{W_y f_y}{\gamma_{M1}} \quad (14)$$

DATA AVAILABILITY STATEMENT

Some or all data, models, or code that support the findings of this study are available from the corresponding author upon reasonable request.

ACKNOWLEDGEMENT

The first author is funded by a PhD fellowship from the Research Foundation Flanders. Furthermore, Outokumpu and Industeel are gratefully acknowledged for providing the stainless steel for this study.

REFERENCES

- Afshan, S. and Gardner, L. 2013. The continuous strength method for structural stainless steel design. Thin-Walled Structures, Volume 68, Pages 42-49.
- Afshan, S., Francis, P., Baddoo, N.R. and Gardner, L. 2015. Reliability analysis of structural stainless steel design provisions. Journal of Constructional Steel Research, Volume 114, Pages 293-304.
- Baddoo, N. 2013. AISC Design guide 27. Structural stainless steel.
- Burgan, B.A., Baddoo, N.R. and Gilsenan, K.A. 2000. Structural design of stainless steel members comparison between Eurocode 3, Part 1.4 and test results. Journal of Constructional Steel Research, Volume 54, Pages 51-73.
- European Committee for Standardization (CEN). 2002. Eurocode 0: Basis of structural design. Brussel, 2002.
- European Committee for Standardization (CEN). 2005. Eurocode 3: design of steel structures - part 1-1: General rules and rules for buildings. Brussel, 2005(+AC:2009)/A1:2014.

394 European Committee for Standardization (CEN). 2006. Eurocode 3: design of steel structures - part 1-4:
 395 General rules - Supplementary rules for stainless steels. Brussel, 2006/A1:2015.

396 Fortan, M., Zhao, O. and Rossi, B. 2016. Lateral torsional buckling of welded duplex stainless steel I section
 397 beams. Proceedings of the Sixth International Conference on Structural Engineering, Mechanics and
 398 Computation 2016. Cape Town, South Africa.

399 Fortan, M. and Rossi, B. 2020. Lateral torsional buckling of welded stainless steel I-profiles: experimental
 400 study. Journal of Structural Engineering. (Under review)

401 Stangenberg H. 2000. Structural design of stainless steel welded I-beams, I-columns and beam-columns.
 402 ECSC Project: Development of the use of stainless steel in construction WP3. Contract no. 7210 SA/134.

403 Steel Construction Institute (SCI). 2017. Design manual for structural stainless steel. 4th edition. SCI
 404 publication P413. SCI, Ascot.

405 Taras, A. and Greiner, R. 2010. New design curves for lateral-torsional buckling - Proposal based on a
 406 consistent derivation. Journal of Constructional Steel Research, Volume 66, pages 648-663.

407 Taras, A. 2011. Contribution to the development of consistent stability design rules for steel members. Graz
 408 University of Technology. PhD thesis.

409 Van Wyk, M.L., Van den Berg, G.J. and Van der Merwe, P. 1990. Lateral torsional buckling strength of doubly
 410 symmetric stain-less steel beams. International Specialty Conference on Cold-Formed Steel Structures, 493-504.

411 Wang, Y.Q., Yang, L., Gao, B., Shi, Y.J. and Yuan, H.X. 2014. Experimental Study of Lateral-torsional
 412 Buckling Behavior of Stainless Steel Welded I- section Beams. International Journal of Steel Structures, 14, 411-
 413 420.

414 Yuan, H.X., Wang, Y.Q., Shi, Y.J. and Gardner, L. 2014. Residual stress distributions in welded stainless steel
 415 sections. Thin-Walled Structures, Volume 79, Pages 38-51.

416

417 Tables:

418 Table 1: The imperfection factor and plateau length for different design methods.

419 Table 2: Comparison of the ultimate loads.

420 Table 3: Validation against (Burgan et al, 2000) and (Stangenberg, 2000).

421 Table 4: Validation on (Wang et al., 2014).

422 Table 5: Overview of the material parameters in the parametric study

423 Table 6: Overview of imperfection factors for each plateau length and each stainless steel family.

424 Table 7: Overview of reliability analysis.

425 Table 8: Reliability analysis for AISC of complete dataset.

426 Table 9: Reliability analysis for AISC for slenderness equal to 0.9 and weighed overstrength.

427 Table 10: recommended design parameters for stainless steel.

429 *Table 1: The imperfection factor and plateau length for different design methods.*

	EN 1993-1-4 Stainless steel	EN 1993-1-1 Carbon steel	Taras & Greiner (2010) Carbon steel
α_{LT}	0.76	h/b ≤ 2: 0.49 h/b > 2: 0.76	0.21
$\bar{\lambda}_0$	0.4	0.2	0.2

430

431

432

Table 2: Comparison of the ultimate loads.

Profile	F _{test} [kN]	F _{FEM} [kN]	F _{FEM} /F _{test}
I159x160Lb1000_EN1.4162	651	650	0.999
I160x160Lb1500_EN1.4162	602	589	0.979
I160x160Lb1800_EN1.4162	545	544	0.998
I212x161Lb1250_EN1.4062	904	894	0.989
I214x162Lb1600_EN1.4062	909	891	0.980
I212x160Lb2000_EN1.4062	754	754	0.999
I260x161Lb1100_EN1.4062	1012	998	0.986
I259x160Lb1100_EN1.4162	1026	1007	0.981
I263x161Lb2000_EN1.4062	969	999	1.031
I260x160Lb2200_EN1.4162	986	984	0.998
I260x160Lb2800_EN1.4162	803	802	0.999
I256x160Lb1300_EN1.4404	573	540	0.942
I253x160Lb2200_EN1.4404	481	483	1.004
		Average	0.991
		COV	0.019

433

434

435

436

Table 3: Validation against (Burgan et al, 2000) and (Stangenberg, 2000).

Profile	L_b	Material	F_{test}	F_{FEM}	F_{FEM}/F_{Test}
160x80	1990	4301	248	240	0.97
160x160	1988	4301	578	565	0.98
160x160	4486	4301	396	428	1.08
160x160	1996	4462	955	1038	1.09
160x160	4493	4462	715	705	0.99
320x160	1492	4301	705	719	1.02
320x160	3994	4301	444	462	1.04
				Average	1.02
				COV	0.044

437

Table 4: Validation on (Wang et al., 2014).

Profile	L_b	Material	F_{test}	F_{FEM}	F_{FEM}/F_{Test}
EI1	1749	4401	184.17	198	1.08
EI2	1598.5	4401	236.54	227	0.96
EI3	1455.5	4401	262.92	264	1.00
EI4	1157.5	4401	333.92	364	1.09
EI5	1056.5	4401	397.04	412	1.04
EI6	956.5	4401	442.68	466	1.05
				Average	1.04
				COV	0.042

438

Table 5: Overview of the material parameters in the parametric study

Material	Family	F_y	E	f_u	n	m	ϵ_u
-	-	N/mm ²	N/mm ²	N/mm ²	-	-	-
EN 1.4016	Ferritic	240	200000	430	14	2.56	0.27
EN 1.4404	Austenitic	220	200000	520	7	2.18	0.58
EN 1.4462	Duplex	460	200000	640	8	3.01	0.28

439

440

441

442

443

444

Table 6: Overview of imperfection factors for each plateau length and each stainless steel family.

$\bar{\lambda}_0$	α_{LT}			M_{FEM}/M_{Pred}	
	Average	Standard deviation	Proposal	Average	COV
Ferritic					
0.2	0.14	0.08	0.27	1.103	0.036
0.3	0.15	0.11	0.34	1.136	0.053
0.4	0.21	0.35	0.78	1.268	0.094
Austenitic					
0.2	0.20	0.10	0.37	1.127	0.037
0.3	0.21	0.17	0.48	1.173	0.049
0.4	0.29	0.16	0.55	1.165	0.064
Duplex					
0.2	0.13	0.06	0.23	1.078	0.038
0.3	0.15	0.08	0.27	1.091	0.040
0.4	0.18	0.08	0.30	1.085	0.051

445

446

Table 7: Overview of reliability analysis for European design rules.

Design rules	$\bar{\lambda}_0$	α_{LT}	b	V_δ	γ_{MI} excluding overstrength	γ_{MI} [min-max] including overstrength
Ferritic						
- EN 1993-1-4	0.4	0.76	1.026	0.118	1.50	1.26 - 1.45
- prEN 1993-1-1	0.2	0.21	1.055	0.036	1.21	1.03 - 1.17
- Proposal	0.2	0.27	1.114	0.035	1.12	0.95 - 1.11
- Alternative proposal	0.2	0.28	1.123	0.036	1.12	0.94 - 1.10
Austenitic						
- EN 1993-1-4	0.4	0.76	0.994	0.095	1.46	1.13 - 1.39
- prEN 1993-1-1	0.2	0.21	1.012	0.045	1.27	1.00 - 1.22
- Proposal	0.2	0.37	1.158	0.038	1.10	0.87 - 1.06
- Alternative proposal	0.2	0.31	1.109	0.035	1.15	0.91 - 1.10
Duplex						
- EN 1993-1-4	0.4	0.76	1.051	0.100	1.38	1.24 - 1.37
- prEN 1993-1-1	0.2	0.21	1.083	0.036	1.15	1.06 - 1.17
- Proposal	0.2	0.23	1.107	0.034	1.12	1.02 - 1.12
- Alternative proposal	0.2	0.25	1.129	0.033	1.10	0.99 - 1.10

Table 8: Reliability analysis for American design rules.

Design rules	M_m	F_m	P_m	V_R	V_Q	ϕ
Ferritic						
- AISC	1.2	1	1.13	0.182	0.19	1.01
- Proposal	1.2	1	1.10	0.068	0.19	1.16
Austenitic						
- AISC	1.3	1	1.05	0.168	0.19	1.05
- Proposal	1.3	1	1.13	0.069	0.19	1.28
Duplex						
- AISC	1.1	1	1.13	0.157	0.19	0.97
- Proposal	1.1	1	1.09	0.068	0.19	1.05

451 *Table 9: Reliability analysis for American design rules for slenderness equal to 0.9 and weighed overstrength.*

Design rules	M_m	F_m	P_m	V_R	V_Q	ϕ
Ferritic						
- AISC	1.09	1	0.94	0.081	0.19	0.89
- Proposal	1.09	1	1.06	0.064	0.19	1.02
Austenitic						
- AISC	1.14	1	0.89	0.087	0.19	0.87
- Proposal	1.14	1	1.11	0.074	0.19	1.10
Duplex						
- AISC	1.05	1	0.97	0.068	0.19	0.89
- Proposal	1.05	1	1.06	0.065	0.19	0.97

452

453 *Table 10: Recommended design parameters per stainless steel family.*

	Ferritic	Austenitic	Duplex
α_{LT} : proposal	0.27	0.37	0.23
α_{LT} : alternative proposal	0.28	0.31	0.25
$\bar{\lambda}_0$	0.2	0.2	0.2
γ_{M1}	1.1	1.1	1.1

454

455

456 Figures:

457 Figure 1: Boundary conditions of the validated finite element model.

458 Figure 2: Comparison of the rotations at the loading points (a) and in the middle of the beam (b) for
459 I263x161Lb2000_EN1.4062.

460 Figure 3: Comparison of the vertical displacement at the loading points $U_{y,LP}$ and the total force - FEM (black)
461 and experiment (grey).

462 Figure 4: Comparison of out-of-plane displacement between DIC and FEM for I260x160Lb2200_EN1.4162

463 Figure 5: Comparison of out-of-plane displacement between DIC and FEM for I260x160Lb2000_EN1.4062

464 Figure 6: Comparison of the vertical mid-span displacement and the total load - FEM (black) and experiment
465 (grey) from (Wang et al., 2014).

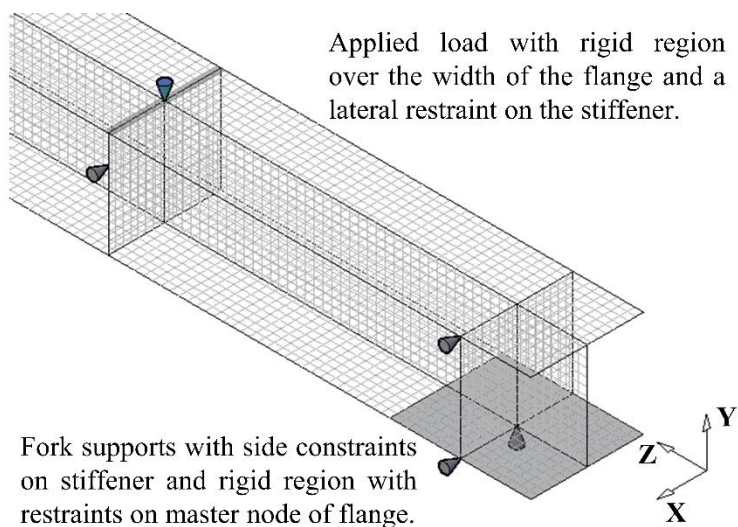
466 Figure 7: Overview of numerical results compared to the buckling curve in EN 1993-1-4.

467 Figure 8: Assessment of the design rules in eurocode for each stainless steel family.

468 Figure 9: Assessment of the design rules in AISC for each stainless steel family

469 Figure 10: Overview of safety factors for all stainless steel families and design rules.

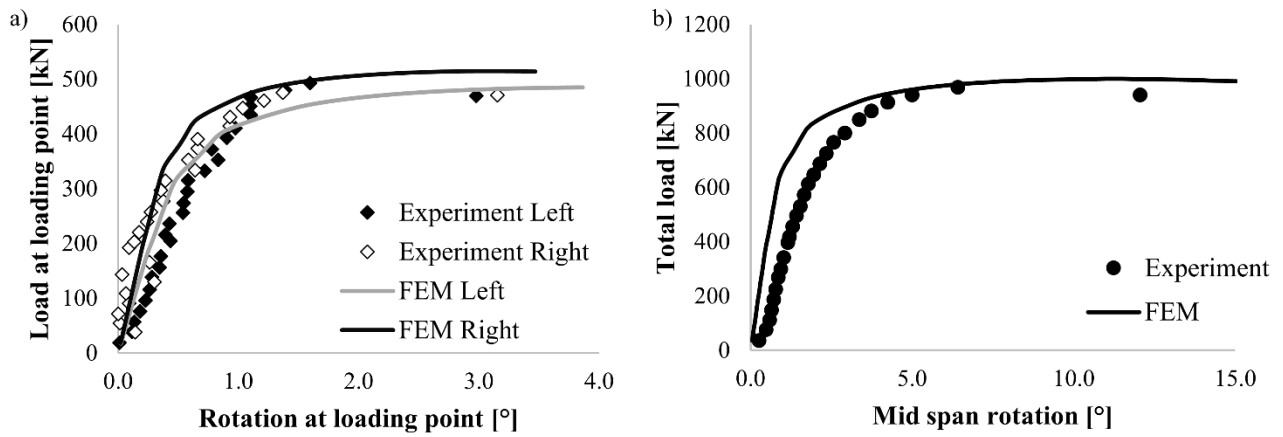
470



471

472 Figure 1: Boundary conditions of the validated finite element model.

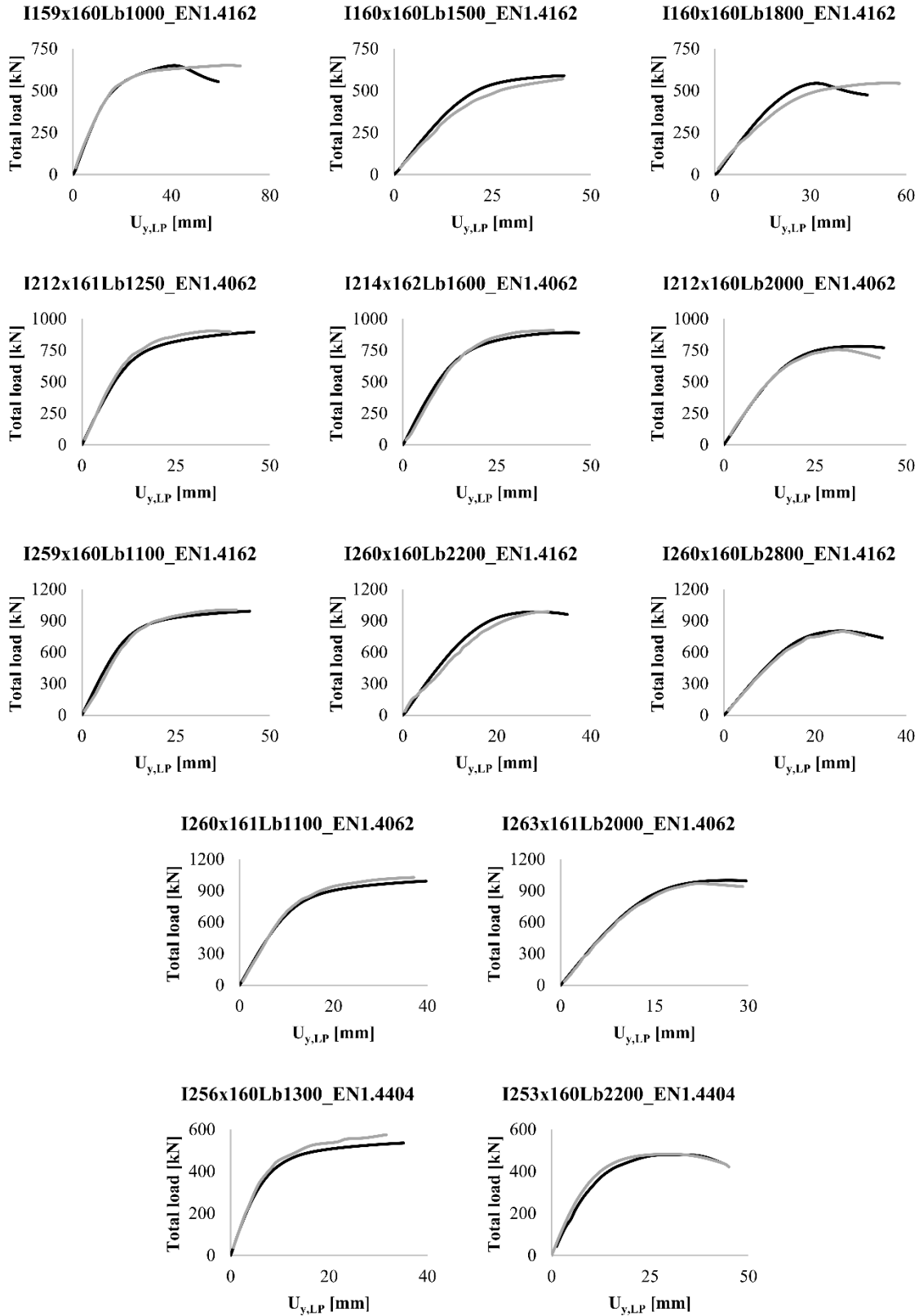
473



474

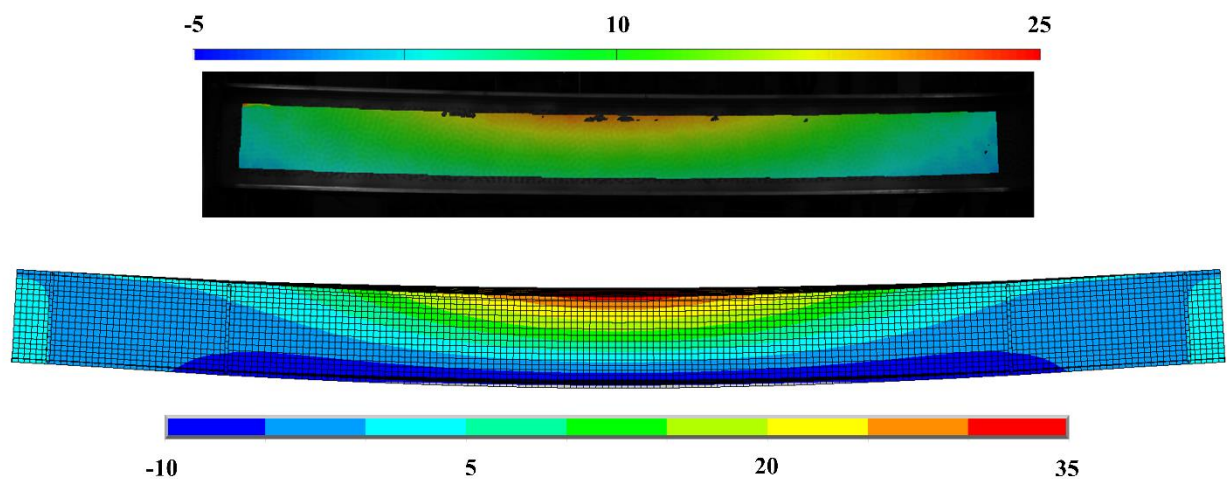
475 Figure 2: Comparison of the rotations at the loading points (a) and in the middle of the beam (b) for
 476 I263x161Lb2000_EN1.4062.

477

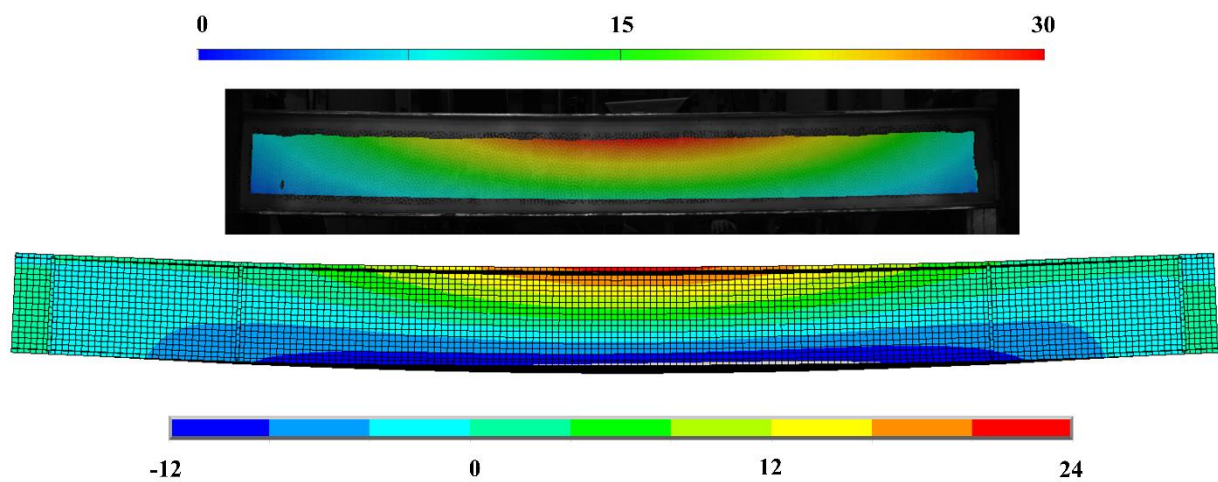


478

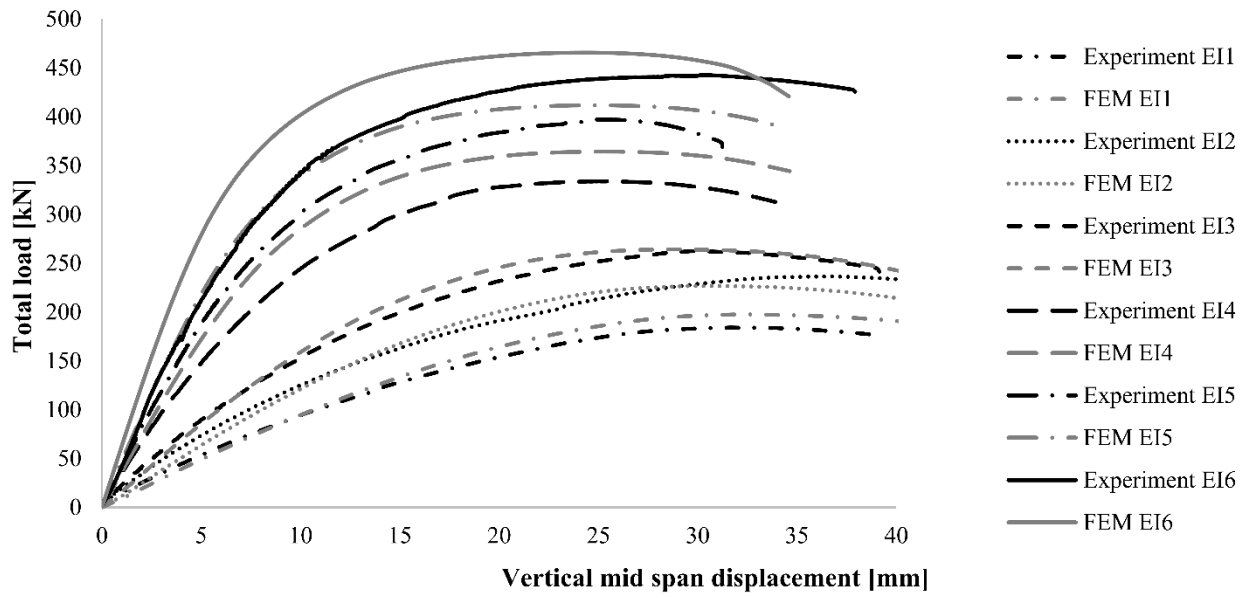
479 Figure 3: Comparison of the vertical displacement at the loading points $U_{y,LP}$ and the total force - FEM (black)
 480 and experiment (grey).



481
482 Figure 4: Comparison of out-of-plane displacement between DIC and FEM for I260x160Lb2200_EN1.4162
483



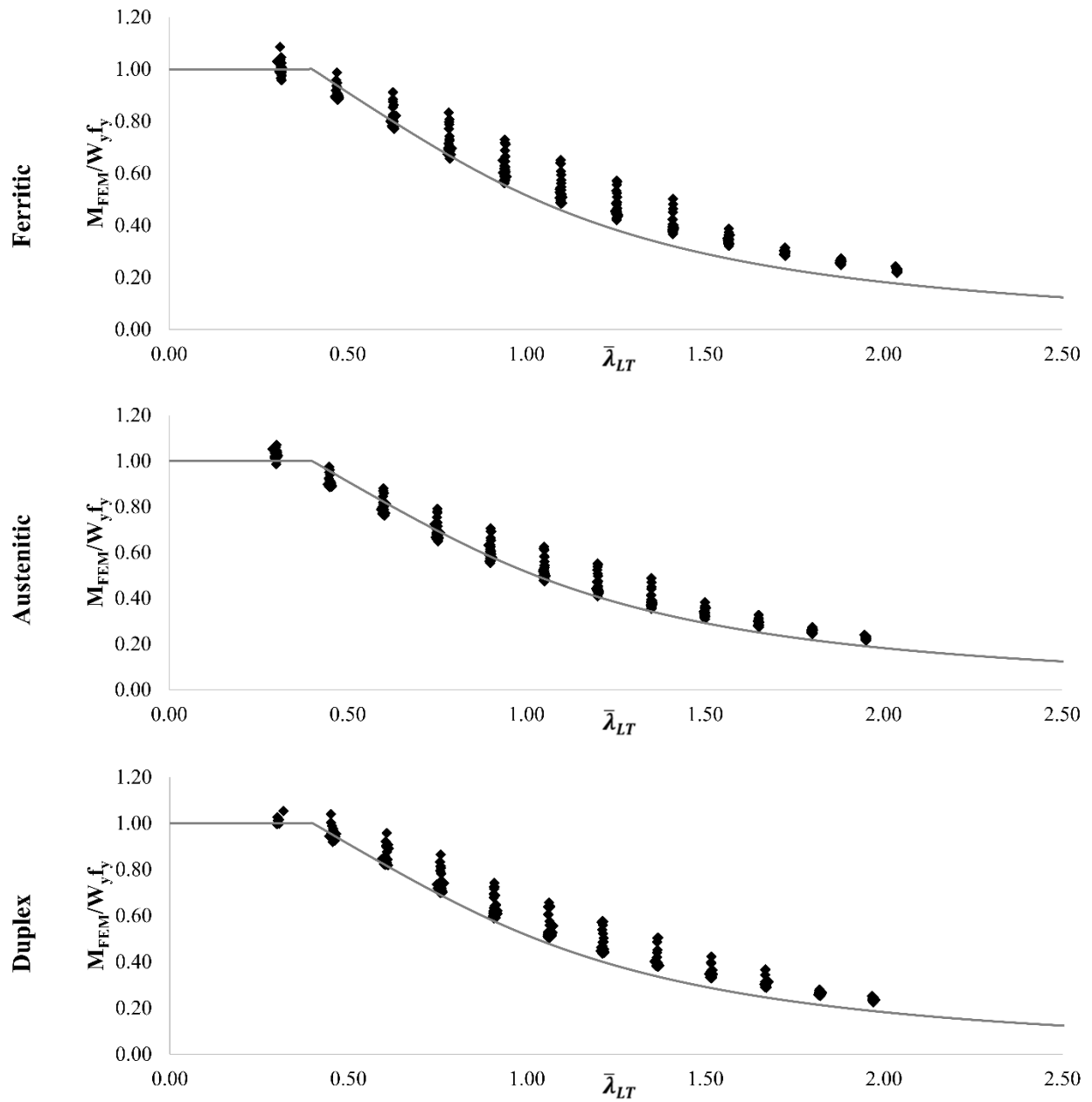
484
485 Figure 5: Comparison of out-of-plane displacement between DIC and FEM for I260x160Lb2000_EN1.4062
486



487

488 Figure 6: Comparison of the vertical mid-span displacement and the total load - FEM (black) and experiment
 489 (grey) from (Wang et al., 2014).

490



491

492 Figure 7: Overview of numerical results compared to the buckling curve in EN 1993-1-4.

493

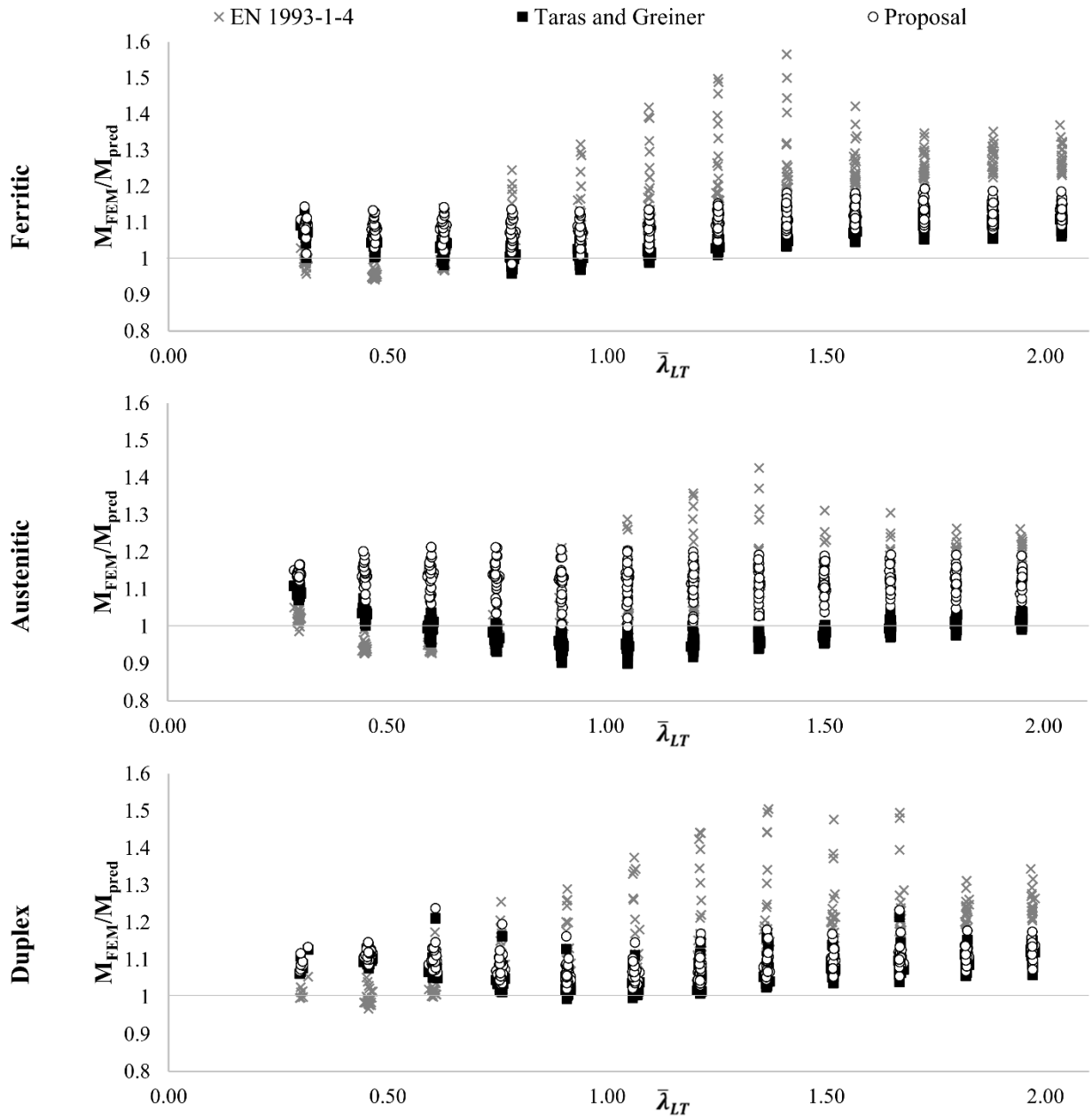


Figure 8: Assessment of the design rules in eurocode for each stainless steel family.

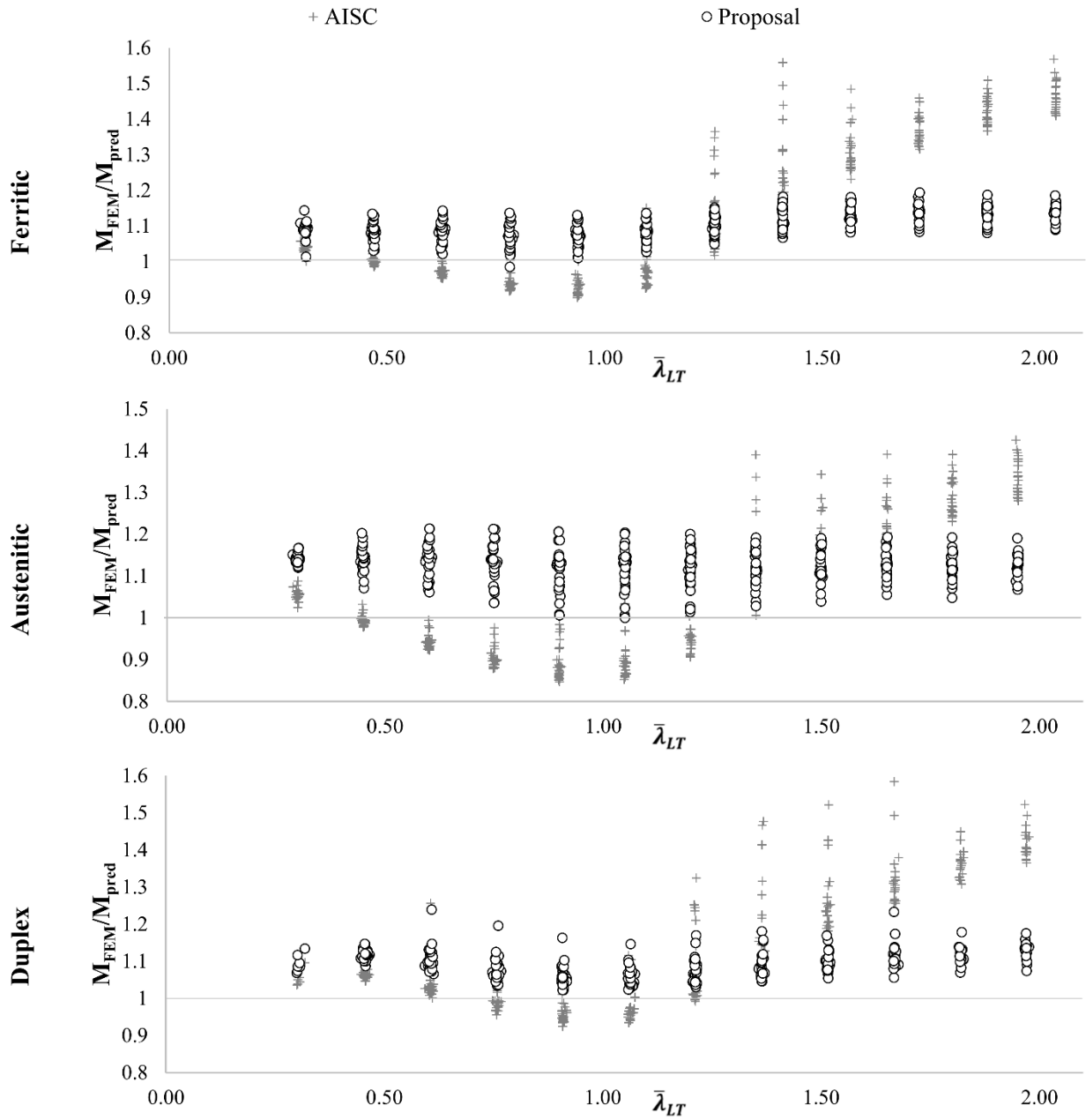


Figure 9: Assessment of the design rules in AISC for each stainless steel family

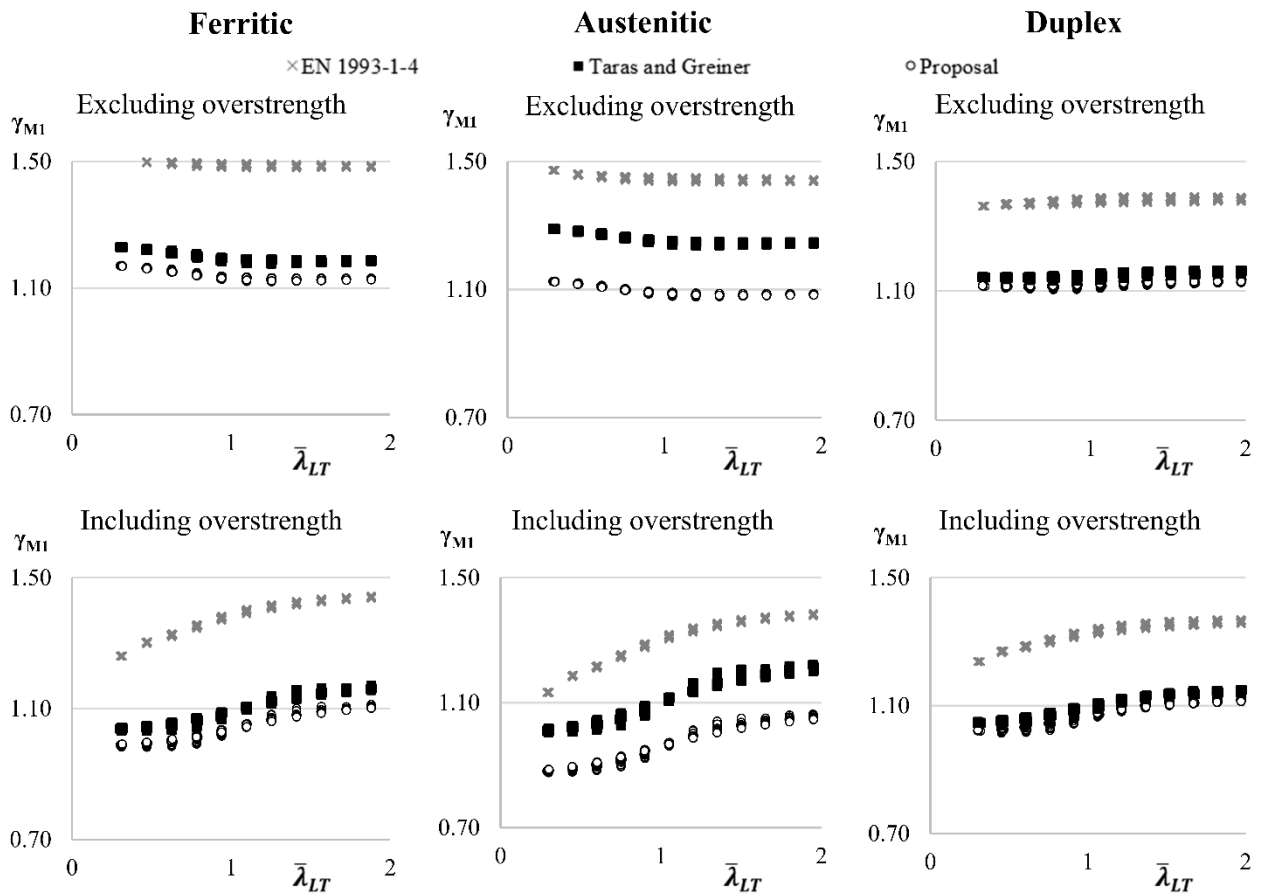


Figure 10: Overview of safety factors for all stainless steel families and design rules.